ChemPubSoc Europe

DOI: 10.1002/chem.201405355

CHEMISTRY
A European Journal
Full Paper

Anhydrous $Pd(NO_3)_2$ and $Pd(CH_3SO_3)_2$

Oxoanionic Noble Metal Compounds from Fuming Nitric Acid: The Palladium Examples $Pd(NO_3)_2$ and $Pd(CH_3SO_3)_2$

Jörn Bruns, Thorsten Klüner, and Mathias S. Wickleder*[a]

Abstract: The oxidation of elemental palladium at 100 °C in a mixture of fuming nitric acid and a pyridine-SO_3 complex leads to the anhydrous nitrate $Pd(NO_3)_2$ (monoclinic, $P2_1/n$, $Z=2$, $a=469.12(3)$ pm, $b=593.89(3)$ pm, $c=805.72(4)$ pm, $\beta=105.989(3)^\circ$, $V=215.79(2)$ Å^3). The Pd^{2+} ions are in square-planar coordination with four monodentate nitrate groups which are connected to further palladium atoms, leading to a layer structure. The reaction of elemental palladium with a mixture of fuming nitric acid and methanesulfonic acid at 120 °C leads to single crystals of $Pd(CH_3SO_3)_2$ (monoclinic, $P2_1/n$, $Z=2$, $a=480.44(1)$ pm, $b=1085.53(3)$ pm, $c=739.78(2)$ pm, $\beta=102.785(1)^\circ$, $V=376.254(17)$ Å^3). Also in this structure the Pd^{2+} ions are in square-planar coordination with four monodentate anions; however, the connection to adjacent palladium atoms leads to a chain-type structure. The thermal decomposition of the compounds has been investigated by means of DSC/TG measurements. Furthermore, IR and Raman spectra have been recorded, and an assignment of the observed vibrational frequencies has been carried out based on theoretical investigations.

Introduction

Over the last years, we have explored reactions of noble metals and noble-metal compounds with highly concentrated mineral acids and their anhydrides under harsh conditions. Under these conditions, unexpected reactivities were frequently observed, and noble metal compounds with unusual structures and properties have been obtained. The gold sulfate $Au_2(SO_4)_2$ is a striking example. The latter forms in the reaction of $Au(OH)_3$ in concentrated sulfuric acid and contains metal–metal-bonded Au_2^{4+} dumbbells.[1] Another interesting example is the reaction of elemental platinum with H_2SO_4 at elevated temperature. Usually platinum is considered to be inert against sulfuric acid, but it turned out that under the conditions applied, the red platinum(III) sulfate $Pt_2(SO_4)_2(HSO_4)_2$ forms. This sulfate also contains a metal–metal bond in the dumbbell-shaped Pt_2^{6+} ion.[2] The lighter platinum congener palladium cannot be oxidized to an oxidation state higher than +II under these conditions and instead the sulfate $PdSO_4$ is found in various modifications.[3] Even with neat SO_3 no high valent palladium can be gained. However, the reaction of palladium with SO_3 afforded a highly remarkable compound, namely the disulfate $Pd(S_2O_7)$.[4] This disulfate exhibits Pd^{2+} ions in unusual octahedral coordination leading to paramagnetic behavior, with low-temperature ferromagnetic ordering of the compound. Interestingly this type of coordination seems to be favored with disulfate groups as ligands, as can be seen from the hydrogendisulfate $Pd(HS_2O_7)_2$, which is also paramagnetic.[5] Up to now, analogous platinum compounds could not be obtained and simple "binary" platinum sulfates are still lacking. However, in the presence of suitable counterions, elemental platinum can be oxidized by oleum to its tetravalent state in form of the complex anion $[Pt(S_2O_7)_3]^{2-}$.[6] The metal atom is coordinated by three chelating disulfate ions, a structural motif that we have observed for a large number of other tetravalent central atoms, such as Si, Ti, Ge, and Sn.[7] Another important focus of our research is the reaction with nitric acid and its anhydride N_2O_5. The latter in particular is an extreme strong oxidizer, and even elemental gold dissolves readily in N_2O_5. This reaction leads to $(NO_2)[Au(NO_3)_4]$ or $(NO)[Au(NO_3)_4]$.[8] As we have shown, these nitrates are interesting precursors for the structuring of elemental gold. Similar compounds could be also obtained for palladium and platinum, namely the complex nitrates $(NO)_2[Pd(NO_3)_4]$ and $(NO)_2[Pt(NO_3)_6]$.[8] In contrast to such nitrato-metalates, binary nitrates of the noble metals are not known up to now; only the hydrate $Pd(NO_3)_2{\cdot}2H_2O$ has been reported.[9] We have now succeeded in the preparation of the first anhydrous noble metal nitrate $Pd(NO_3)_2$ by using a reaction of elemental palladium with fuming nitric acid. This acid is obviously both a strong oxidizer and a suitable solvent for the crystallization of the nitrate. The addition of a small amount of SO_3 (in form of its pyridine complex) to the reaction mixture was thought as a scavenger for H_2O that might form in the reaction. The successful use of fuming nitric acid as a solvent forced us to also investigate the formation of other oxoanionic palladium compounds from that solvent. In course of these attempts we were able to prepare the methanesulfonate

[a] J. Bruns, Prof. Dr. T. Klüner, Prof. Dr. M. S. Wickleder
Carl von Ossietzky Universität Oldenburg
Institut für Chemie
Carl-von-Ossietzky Strasse 9–11
26129 Oldenburg (Germany)
Fax: (+49) 441-798-3352
E-mail: mathias.wickleder@uni-oldenburg.de

Supporting information for this article is available on the WWW under http://dx.doi.org/10.1002/chem.201405355.

$Pd(CH_3SO_3)_2$ when excess methanesulfonic acid was added to the reaction mixture. This compound is the first binary noble metal methanesulfonate reported to date. Furthermore, apart from the gold complexes $M[Au(CH_3SO_3)_4]$ (M = Li, Na, Rb), it is only the second noble metal methanesulfonate at all.[10] This is remarkable because methanesulfonic acid is a very common electrolyte for electroplating, and is also used for such processes involving noble metals.[11] The two palladium compounds have been not only characterized by means of single-crystal X-ray diffraction, but also by thermal analyses, and vibrational spectroscopy supported by quantum chemical calculations.

Results and Discussion

Crystal structures

The anhydrous nitrate $Pd(NO_3)_2$ crystallizes with monoclinic symmetry (Table 1). The Pd^{2+} cation is located on the special Wyckoff site *2b* of space group $P2_1/n$, bearing inversion symmetry. Four oxygen atoms surround it in a square-planar manner with the distances Pd–O being 200.5(1) and 202.5(1) pm, respectively (Figure 1). The angles O-Pd-O of 87.94(4)° and 92.06(4)° show that there is only a slight deviation from ideal values. The observed values for the bond lengths and angles are in good accordance with the values found for the comparable ternary palladium nitrates $M_2[Pd(NO_3)_4]$ (M = Na, K, Rb, Cs, NO).[8,12] The oxygen atoms belong to four monodentate nitrate groups and each nitrate group is connected to one further Pd^{2+} ion leading to infinite layers according to the Niggli formula $^2_\infty[Pd(NO_3)_{4/2}]$ (Figure 2). Within the nitrate group, the Pd^{2+} bonded oxygen atoms show significantly longer N–O distances (127.8(2) and 129.3(2) pm) than the respective distance to the remaining non-coordinating oxygen atom (120.7(2) pm). The observed distances match very well the respective data obtained for theoretical investigations (see caption of Figure 1). These have been performed on the fragment $[(NO_3)_3Pd(NO_3)Pd(NO_3)_3]^{3-}$ as a cut-off of the three-dimensionally linked crystal structure. This fragment is used as a suitable model for the bidentate bridging nitrate group. The infinite

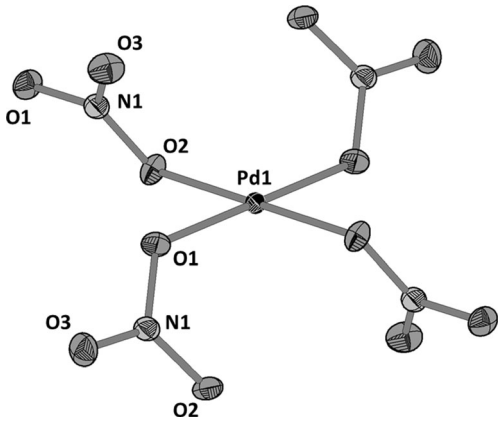

Figure 1. Structure and atom labeling for the $[Pd(NO_3)_4]$ unit in $Pd(NO_3)_2$. The four nitrate anions are related by inversion symmetry at the Pd site. Ellipsoids are set at 75% probability. Selected bond lengths [pm] and angles [°] (theoretical values in italics): Pd1–O1 200.5(1)/*204.3*, Pd1–O2 202.5(1)/*209.4*, N1–O1 127.8(2)/*128.3*, N1–O2 129.3(2)/*128.4*, N1–O3 120.7(2)/*122.4*, O1-Pd1-O2 87.94(4)/*89.3*, O2-Pd1-O1 92.06(4)/*91.6*, O1-N1-O2 117.2(1)/*118.6*, O1-N1-O3 119.8(1)/*119.1*, O2-N1-O3 124.0(1)/*122.3* (For a full list, see the Supporting Information, Table S3).

Table 1. Crystal data and structure refinement for $Pd(NO_3)_2$ and $Pd(CH_3SO_3)_2$.

Formula	$Pd(NO_3)_2$	$Pd(CH_3SO_3)_2$
Formula weight [gmol^{-1}]	230.42	296.59
Temperature [K]	153(2)	120(2) K
Crystal system	monoclinic	monoclinic
Space group	$P2_1/n$ (No. 14)	$P2_1/n$ (No. 14)
a [pm]	469.12(3)	480.44(1)
b [pm]	593.89(3)	1085.53(3)
c [pm]	805.72(4)	739.78(2)
β [°]	105.989(3)	102.785(1)
Volume [Å^3]	215.79(2)	376.25(2)
Z	2	2
ρ_{calc} [mg m^{-1} m^3]	3.546	2.618
Absorption coefficient [cm^{-1}]	42.58	30.01
F(000)	216	288
Crystal size [mm^3]	0.05×0.02×0.02	0.18×0.08×0.06
2θ range for data collection	8.64 to 80.54°	6.782 to 80.558°
Index ranges	$-8 \le h \le 8$	$-8 \le h \le 8$
	$-10 \le k \le 10$	$0 \le k \le 19$
	$-14 \le l \le 14$	$0 \le l \le 13$
Reflections collected	12002	15247
Independent reflections	1368 (R_{int} = 0.0354)	3994 (R_{int} = 0.0224)
Completeness to θ = 40.27°	1.000	0.999
Absorption correction	empirical	multi-scan
Refinement method	Full-matrix least-squares on F^2	Full-matrix least-squares on F^2
Data/restraints/parameters	1368/0/44	3994/0/54
Goodness-of-fit on F^2	1.051	1.070
Final *R* indexes [$I \ge 2\sigma(I)$]	R_1 = 0.0159, wR_2 = 0.0316	R_1 = 0.0150; wR_2 = 0.0416
Final *R* indexes (all data)	R_1 = 0.0288, wR_2 = 0.0346	R_1 = 0.0161; wR_2 = 0.0421
Extinction coefficient	0.0077(11)	–
Largest diff. peak/hole/e$^-$/Å^{-3}	0.50/−0.63	0.54/−102
Ratio of non-meroedric twin individuals [%]		47:53
Deposition number	425998 (see *ICSD*)	963236 (see *CCDC*)

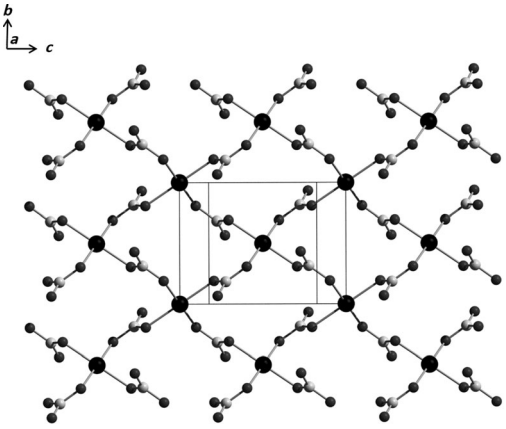

Figure 2. Infinite layers according to $^2_\infty[Pd(NO_3)_{4/2}]$ in the structure of $Pd(NO_3)_2$. The layers are oriented parallel to the (−101) plane of the unit cell.

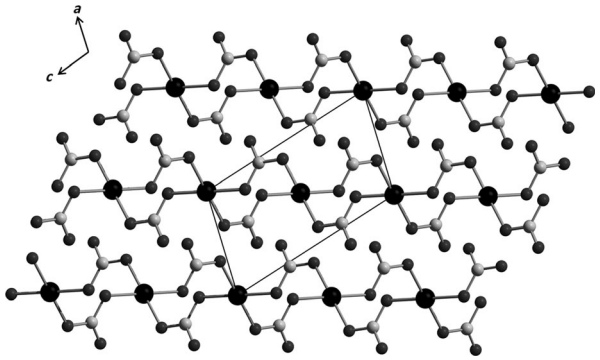

Figure 3. View of the layers shown in Figure 2 along the [010] direction. The layers are held together only by weak interactions.

layers of nitrate linked Pd^{2+} cations are oriented parallel to the ($\bar{1}01$) plane of the unit cell (Figure 3). The layers are held together by weak interactions only. The shortest distances between palladium atoms and oxygen atoms of adjacent layers are clearly above 350 pm.

Similar to the structure of $Pd(NO_3)_2$, in the monoclinic methanesulfonate $Pd(CH_3SO_3)_2$ the Pd^{2+} ion is also located on a special position with inversion symmetry of the space group $P2_1/n$ (Wyckoff site *2a)* and coordinated in a square planer manner by oxygen atoms (Figure 4). The Pd–O distances show typical values of 201.16(8) and 202.05(8) pm and the [PdO_4] moiety is, with respect to the angles O-Pd-O of 94.17(3) and 85.83(3)°, slightly more distorted compared to the structure of $Pd(NO_3)_2$.

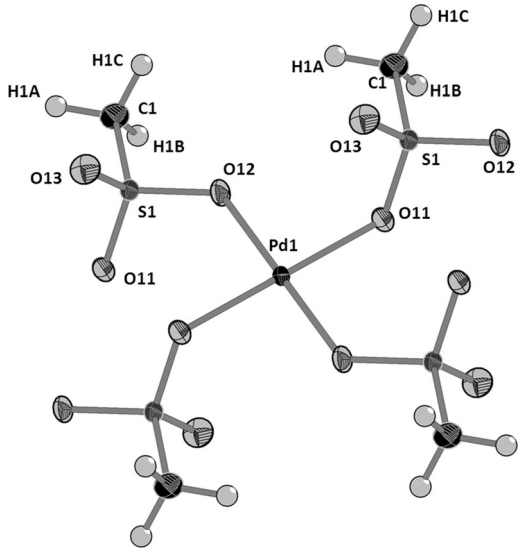

Figure 4. Structure and atom labeling of the [$Pd(CH_3SO_3)_4$] unit in $Pd(CH_3SO_3)_2$. Ellipsoids are set at 75% probability. Selected bond lengths [pm] and angles [°] (theoretical values in italics): Pd1–O11 200.16(8)/*203.2*, Pd1–O12 202.05(8)/*206.5*, S1–O11 150.02(8)/*152.3*, S1–O12 149.09(8)/*152.1*, S1–O13 143.54(9)/*147.1*, S1–C1 174.98(11)/*179.6*, O1-Pd1-O2 85.83(3)/*87.8*, O2-Pd1-O1 94.17(3)/*90.8*, O11-S1-O12 107.47(5)/*112.4*, O11-S1-O13 113.30(5)/*115.7*, O11-S1-C1 106.03(5)/*102.8*, O12-S1-O13 114.77(5)/*110.7*, O12-S1-C1 103.68(5)/*105.7*, O13-S1-C1 110.81(5)/*108.7* (for a full list, see the Supporting Information, Table S3).

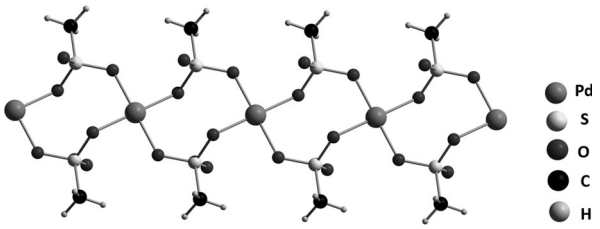

Figure 5. Infinite chains according to the *Niggli* formula $^1_\infty[Pd(CH_3SO_3)_{4/2}]$ in the structure of $Pd(CH_3SO_3)_2$.

The oxygen atoms belong to four monodentate $CH_3SO_3^-$ anions, which are connected to one further Pd^{2+} ion. In contrast to the structure of $Pd(NO_3)_2$, this connection leads now to a chain structure according to $^1_\infty[Pd(CH_3SO_3)_{4/2}]$ (Figure 5). Those oxygen atoms of the anion that are connected to a palladium cation show significantly longer S–O bonds (149.09(8) and 150.02(8) pm) compared to the uncoordinated oxygen atom (143.54(9) pm). This finding is expected and in line with the observation for the $[Au(CH_3SO_3)_4]^-$ complex, which shows even a distance of about 154 pm for the gold-coordinated oxygen atom.[10] Furthermore, the observed distances are well reproduced by theory (cf. caption of Figure 4). For these calculations the $[(CH_3SO_3)_2Pd(CH_3SO_3)_2Pd(CH_3SO_3)_2]^{2-}$ fragment has been chosen as a model. It is essentially a part of the $^1_\infty[Pd(CH_3SO_3)_{4/2}]$ chain. These $^1_\infty[Pd(CH_3SO_3)_{4/2}]$ chains in $Pd(CH_3SO_3)_2$ are oriented along the [100] direction and they are related by the glide plane *n* that is perpendicular to the [010] direction at $y = {}^1/_4$[010] (Figure 6). The chains are arranged in a typical densest rod-packing fashion, and there are obviously only weak interactions between the chains. These might be attributed to hydrogen bridges with CH_3 groups as donor groups and the non-coordinated oxygen atoms of sulfonate groups as acceptors. Even if this type of hydrogen bridge is certainly very weak, they are believed to be important for the assembling of neutral building blocks in the solid state.[13] The shortest donor–acceptor distances are found between C1

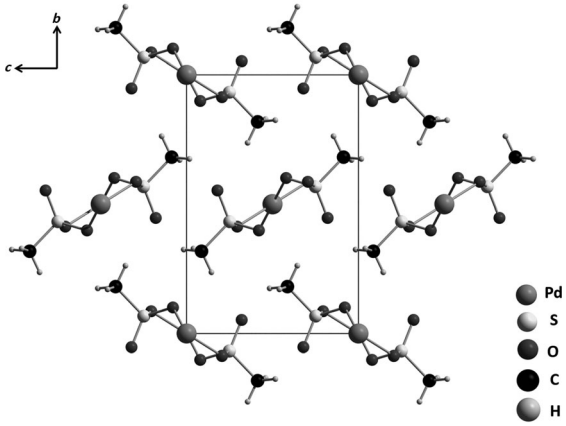

Figure 6. The $^1_\infty[Pd(CH_3SO_3)_{4/2}]$ chains in $Pd(CH_3SO_3)_2$, which are arranged in a rod-packing fashion along the [100] direction. They are related by the glide plane *n* of the monoclinic unit cell.

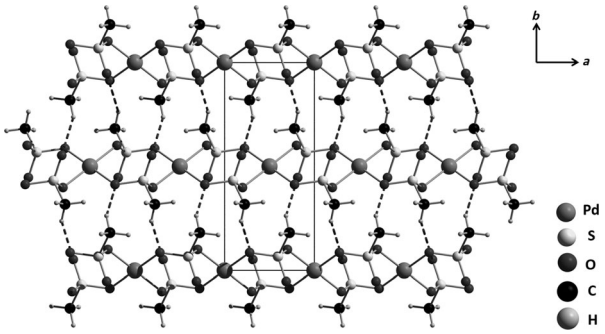

Figure 7. Weak hydrogen bonds between the $^{1}_{\infty}[Pd(CH_3SO_3)_{4/2}]$ chains in $Pd(CH_3SO_3)_2$. The donor–acceptor distance for the bridges emphasized by dashed lines is 344.3(1) pm.

and O13 at 344.3(1) pm (Figure 7), that is, very weak according to Jeffrey's nomenclature.[14]

Thermal behavior

According to the DSC/TG measurement, the thermal decomposition of $Pd(NO_3)_2$ occurs in a two-step process (Figure 8). A slight mass loss of about 3% at the beginning of the thermal treatment can be attributed to remains of the solvent (*n*-hexane) that was used during sample preparation. $Pd(NO_3)_2$ starts to decompose with an onset temperature of 165 °C (Table 2). This first decomposition step ends at 275 °C (T_{max} = 247 °C) and is accompanied by an experimental mass loss of 46.7%, in accordance with the loss of one molecule of N_2O_5 per formula unit. As intermediate the oxide PdO is formed, as has been proven by XRD measurements. The degradation of $Pd(NO_3)_2$ matches quite well our observations during the decomposition of $(NO)_2[Pd(NO_3)_4]$. For this compound, we postulated the intermediary formation of anhydrous $Pd(NO_3)_2$, which then is further decomposed to PdO at a temperature of 168 °C, in accordance with the findings presented here. The final step is the decomposition of PdO, yielding elemental palladium. This decomposition occurs between 640 and 760 °C (T_{max} = 740 °C) accompanied by an experimental mass loss of 7.3% (calcd. 6.9%). The nature of the residue as elemental palladium has also been confirmed by XRD techniques (Supporting Information, Figure S6).

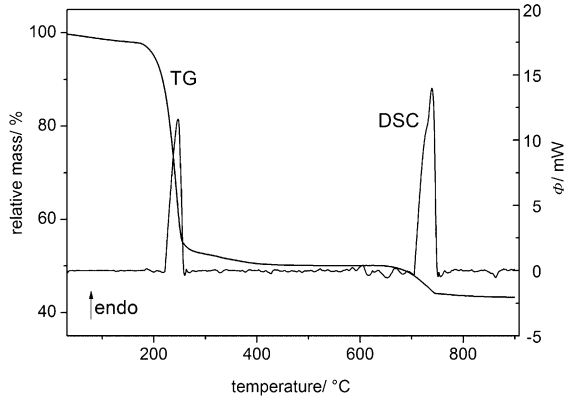

Figure 8. DSC/TG diagram of the thermal decomposition of $Pd(NO_3)_2$. Up to 150 °C there is a small mass loss, which can be attributed to the evaporation of adhesive solvent.

Table 2. Experimental and calculated mass loss of the thermal decomposition of $Pd(NO_3)_2$ with confirmed intermediary and final products.

Step	$T_{onset}/T_{max}/T_{end}$	Mass loss (exp.) [%]	Mass loss (calc.) [%]	Product
1	165/247/275	46.7	46.9	PdO
2	640/740/760	7.3	6.9	Pd
Σ		54.0	53.8	Pd

The thermal decomposition of $Pd(CH_3SO_3)_2$ has been monitored in both a flowing stream of nitrogen and oxygen, respectively, in the temperature range from 25 to 1050 °C (Figure 9). In both cases, the first mass loss observed can be attributed to some adhesive CH_3SO_3H that could not be removed completely during the sample preparation. The decomposition of the methanesulfonate occurs nearly in the same temperature region, independent of the nature of the gas stream (Table 3). In both cases, two closely related signals are observed in the DSC curve. However, while under N_2 atmosphere the decomposition is endothermic, the process is clearly exothermic under O_2 conditions. The first decomposition is accompanied by an experimental mass loss of 28.4%, the second by about

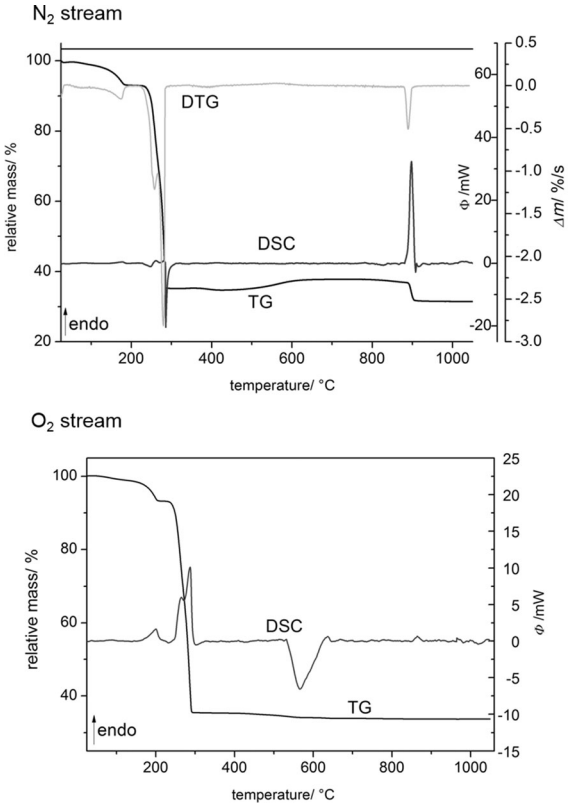

Figure 9. DSC/TG analysis of $Pd(CH_3SO_3)_2$ in N_2 (top) and O_2 (bottom) atmosphere, respectively. In both cases there is a significant mass loss which can be attributed to the removal of adhesive CH_3SO_3H.

Table 3. Experimental and calculated mass loss of the thermal decomposition of $Pd(CH_3SO_3)_2$ with proved final product.

N_2 stream				
Step	Onset/T_{max}/offset	Mass loss (exp.) [%]	Mass loss (calc.) [%]	Product
1	230/265/270	28.4		
2	270/290/310	33.6		
Σ		62.0	64.1[a]	Pd
O_2 stream				
Step	Onset/T_{max}/offset	Mass loss (exp.) [%]	Mass loss (calc.) [%]	Product
1	225/255/270	27.9		
2	270/280/310	34.2		Pd
3[b]	820/849/890			Pd
Σ		62.1	64.1[a]	Pd

[a] For the calculation the mass of the sample after removal of adhesive solvent is set to 100%. [b] Prior to the decomposition of PdO this oxide forms in the reaction of Pd in the oxygen stream.

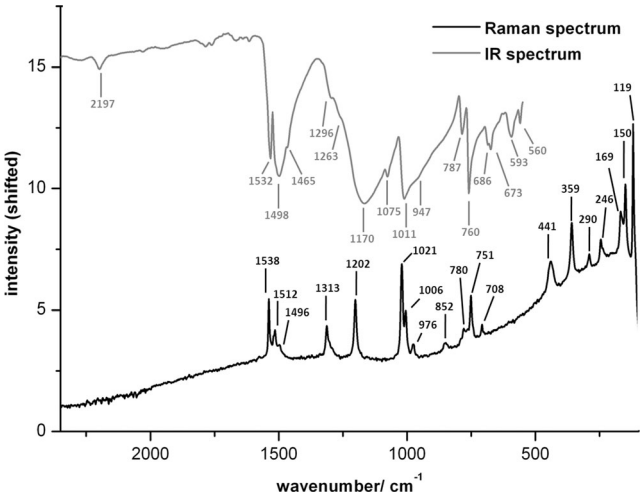

Figure 10. IR spectrum (top) and Raman spectrum (bottom) of $Pd(NO_3)_2$.

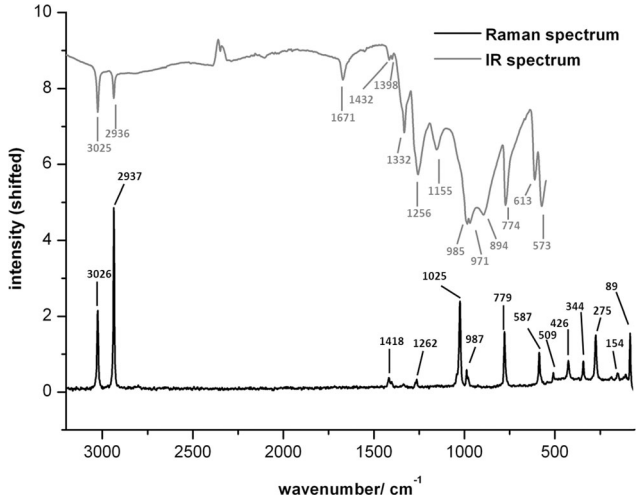

Figure 11. IR spectrum (top) and Raman spectrum (bottom) of $Pd(CH_3SO_3)_2$.

33.6% (N_2 atmosphere; both scaled to the solvent-free starting material at 210 °C). The decomposition product in both cases is elemental palladium. For the investigations under oxygen atmosphere, the mass of the sample increases in the temperature region between 495 and 620 °C. This is due to the formation of PdO, which again decomposes at higher temperature to elemental palladium. To test this assumption, we have performed a comparable measurement of palladium metal in an O_2 stream. We actually found the same signature as discussed before (Supporting Information, Figure S5). In any case, the formation of palladium metal as the final decomposition residue has been confirmed by XRD measurements.

It is remarkable that in both cases the decomposition of $Pd(CH_3SO_3)_2$ leads directly to elemental palladium, in contrast to the findings for $Pd(NO_3)_2$, where PdO is the primary degradation compound. Obviously the $CH_3SO_3^-$ anion is a suitable reductant during the decomposition.

Vibrational spectroscopy

The vibrational spectra of $Pd(NO_3)_2$ and $Pd(CH_3SO_3)_2$ are quite complex (Figures 10 and 11). To assure a reasonable assignment of the observed bands, we used the calculations on the fragments $[(NO_3)_3Pd(NO_3)Pd(NO_3)_3]^{3-}$ and $[(CH_3SO_3)_2Pd(CH_3SO_3)_2Pd(CH_3SO_3)_2]^{2-}$, respectively. As expected, most of the observed bands are combination modes also involving the $[PdO_4]$ moieties. However, some of the vibrational modes can be attributed quite clearly. The observed bands and their assignments are collected in Table 4.

For $Pd(NO_3)_2$, the vibration bands with the highest energies are observed around 1500 cm^{-1}. According to the DFT calculations, these bands can be clearly attributed to N=O stretching vibrations involving the non-coordinating oxygen atoms of the nitrate group. This energy is clearly above the value for a bare NO_3^- ion (1340 cm^{-1}), for example in anilinium nitrate,[15] and demonstrates the double bond character expected for the third oxygen atom of the bidentate bridging nitrate ion. The N–O vibrations involving the palladium-coordinated oxygen atoms are at about 1300 cm^{-1} for the asymmetric and between 1000 and 1200 cm^{-1} for the symmetric modes. However, these latter modes are already affected by Pd–O vibrations of the $[PdO_4]$ moiety. The Pd–O vibrations became even dominant for the bands observed between 1000 and 850 cm^{-1}. At energies below 800 cm^{-1}, the vibration modes are essentially stamped by the in-plane and out-of-plane bending modes of the nitrate group. The measuring range of the Raman spectrum allows also for the detection of several lattice modes, which occur between 119 and 441 cm^{-1}. One additional band in the IR spectrum at 2197 cm^{-1} is not assignable. We believe that trace residues of nitric acid cause the presence of some NO species, which have the strongest vibration around this value.[16]

The IR and the Raman spectra show a large number of mainly characteristically resolved bands for the methanesulfonate as well (Figure 11, Table 5). The band distribution of

Table 4. IR frequencies and their assignment for $Pd(NO_3)_2$.[a]

IR frequency [cm^{-1}]		Raman[b] frequency [cm^{-1}]		Assignment
560	w			
593	m			δ $(NO_3)_{out\text{-}of\text{-}plane}$
673	m	636	w	
686	sh	708	w	
760	s	751	m	δ $(NO_3)_{in\text{-}plane}$
787	m	780	w	
		852	w	ν (N–O)+ν (Pd–O)
947	sh	976	w	
		1006	m	
1011	s	1021	s	
1075	m		s	ν_s $(N–O_{coord.})$
1170	s	1202	s	
1263	sh		w	ν_{as} $(N–O_{coord.})$
1296	w	1313	m	
1465	sh	1496	w	
1498	sh	1512	m	ν $(N{=}O_{unc})$
1532	sh	1538	s	

[a] s = strong, m = medium, w = weak, sh = shoulder. [b] In the Raman spectrum, there are additionally some lattice vibrations in the range between 119 and 441 cm^{-1} visible (cf. Figure 10).

Table 5. IR frequencies and their assignment for $Pd(CH_3SO_3)_2$.[a]

IR frequency [cm^{-1}]		Raman[b] frequency [cm^{-1}]		Assignment
		509	w	
573	s			δ (SO_3)
613	m	587	m	
774	s			
		779	s	ν (S–C)
894	m			
971	m			
985	m	987	m	ν (S–O)+ν (Pd–O)
		1025	s	
1155	m			
1256	s	1262	w	ν_{as} $(S–O_{coord.})$
1332	m			
1398	w			
1432	w	1418		ν_{as} $(S–O_{unc.})$
2936		2937	s	ν_s (C–H)
3025		3026	s	ν_{as} (C–H)

[a] s = strong, m = medium, w = weak, sh = shoulder. [b] In the Raman spectrum, there are additionally some lattice vibrations in the range between 89 and 426 cm^{-1} visible (cf. Figure 11).

the IR spectrum fits very well to those of recently presented ternary gold methanesulfonates $Li[Au(CH_3SO_3)_4]$ and $Rb[Au(CH_3SO_3)_4]$,[10] the only previous examples of precious metal methanesulfonates. The findings for previously reported alkaline earth methanesulfonates of sodium and cesium also fall in the narrow range of the results for $Pd(CH_3SO_3)_2$. Each spectrum reveals significant strong signals at high wavenumbers in the IR as well as in the Raman spectra. The bands of highest energy are found at 3025 and 2936 cm^{-1} in the IR and 3026 cm^{-1} and 2937 cm^{-1} in the Raman spectrum. With respect to our calculations and in accordance with reported data, they can be clearly attributed to the asymmetric and symmetric C–H stretching modes. At energies between 1450 and 1150 cm^{-1} the S–O stretching modes are seen. They can be separated into those vibrations that involve terminal non-coordinated oxygen atoms (1398–1432 cm^{-1}) and those that involve palladium-coordinated oxygen atoms (1155–1332 cm^{-1}). The latter are influenced by Pd–O modes of the $[PdO_4]$ fragment, similar to the findings for $Pd(NO_3)_2$. Also in line with the observations for the nitrate, the bands between 894 and 1025 cm^{-1} are clearly dominated by Pd–O vibrations. Another strong band occurs at about 770 cm^{-1} in both spectra, which can be assigned to the S–C stretching modes. Finally, the deformation vibrations of the $CH_3SO_3^-$ anion are found between 509 and 613 cm^{-1}. Low-energy bands between 89 and 426 cm^{-1} in the Raman spectrum are due to lattice vibrations. There is one band at 1673 cm^{-1}, which could not be assigned reliably.

Conclusion

We have demonstrated for the first time that fuming nitric acid might be a suitable reactant and also a solvent for the preparation of oxoanionic noble metal compounds. This is of outstanding importance because these type of compounds have been only scarcely investigated owing to lacking synthetic methods for their preparation. The reported representatives are the palladium compounds $Pd(NO_3)_2$ and $Pd(CH_3SO_3)_2$ exhibiting a layer and a chain structure, respectively. We are convinced that the preparation route will lead to further noble metal compounds of this kind in the future.

Experimental Section

Synthesis of $Pd(NO_3)_2$

Pd (0.055 g (0.52 mmol), Hereaus, Hanau, Germany) and the pyridine-SO_3 complex (0.095 g, 0.60 mmol), Merck, Darmstadt, Germany) were loaded into a thick-walled glass ampoule (length 250 mm, diameter 20 mm, thickness of the tube wall 2 mm). Fuming nitric acid (1.5 mL; Merck, Darmstadt, Germany) was added. The ampoule was torch-sealed, placed into a tube furnace, and heated up to 100 °C. The temperature was maintained for 30 h and finally decreased to 25 °C via 150 h. A large number of yellow crystals were obtained, and the yield was quantitative with respect to the initial palladium. The product was handled under strictly inert conditions. **Caution!** Fuming nitric acid is a strong oxidizer, which needs careful handling. During and even after the reaction the ampoule might be under remarkable pressure and contains nitrous fumes. It is mandatory to cool down the ampoules with liquid nitrogen prior to opening.

Synthesis of $Pd(CH_3SO_3)_2$

Elemental palladium (100 mg, 0.94 mmol), Hereaus, Hanau, Germany), was loaded into a thick-walled glass ampoule (length 250 mm, diameter 20 mm, thickness of the tube wall = 2 mm). After adding fuming nitric acid (1 mL; Merck, Darmstadt, Germany) and methanesulfonic acid (2 mL; Sigma Aldrich, Steinheim, Germany) the ampoule was torch-sealed, placed into a block resistance furnace, and heated up to 120 °C within 24 h. The temperature was maintained for 72 h, additionally the temperature was decreased to 25 °C in a two-step process, first within 79 h to 50 °C and finally to 20 °C

within 50 h. Additionally, the ampoule was left unchanged for crystallization at room temperature for 70 days. Finally, a large number of yellow crystals were obtained, and the yield was quantitative with respect to the initial palladium. The crystals are extremely moisture sensitive. Therefore the crystals have to be handled under strictly inert conditions. **Caution!** Fuming nitric acid and methanesulfonic acid are strong oxidizers which need careful handling. During and even after the reaction the ampoules might be under remarkable pressure. It is mandatory to cool down the ampoules by liquid nitrogen prior to opening.

X-ray crystallography

Several single crystals were transferred into inert oil (AB128333, ABCR, Karlsruhe, Germany). A suitable crystal was prepared, mounted onto a glass needle (diameter 0.1 mm) and immediately placed into a stream of cold N_2 (120 K) inside the diffractometer (κ-APEX II, Bruker, Karlsruhe, Germany). After unit-cell determination, the reflection intensities were collected. Structure solution and refinements were done with the SHELX program package.[17]

The crystal structure of $Pd(NO_3)_2$ could be solved in the monoclinic space group $P2_1/n$ (no. 14). The heavy atom positions were determined by SHELXS-97 using direct methods.[17] Further atoms could be successfully located by difference Fourier techniques during refinement with SHELXL-97.[17] An absorption correction was applied to the data using the program SADABS-2012/1.[18] Finally the structure and model refined to $R_1 = 0.0288$ and $wR_2 = 0.0346$ for all data. Selected bond lengths are presented in the Supporting Information, Table S4. For $Pd(NO_3)_2$, further details of the crystal structure investigation may be obtained from the Fachinformationszentrum Karlsruhe, 76344 Eggenstein-Leopoldshafen, Germany (Fax: (+49) 7247-808-666; e-mail: crysdata@fiz-karlsruhe.de, or at http://www.fiz-karlsruhe.de/request_for_deposited_data.html) on quoting the CSD number 425998. CCDC 963236 ($Pd(CH_3SO_3)_2$) contain the supplementary crystallographic data for this paper. These data can be obtained free of charge from The Cambridge Crystallographic Data Centre via www.ccdc.cam.ac.uk/data_request/cif.

The crystal structure of $Pd(CH_3SO_3)_2$ could be solved in the monoclinic space group $P2_1/n$ (no. 14). The heavy-atom positions were determined by SHELXS-2013 using direct methods.[17] Further atoms could be successfully located by difference Fourier techniques during refinement with SHELXL-2013.[17] The investigated crystal was calculated as non-meroedric twin and the ratio of the two individuals was found to be 47%/53%. An absorption correction was applied to the data using the program TWINABS-2012/1.[19] Finally the structure and model refined to $R_1 = 0.0161$ and $wR_2 = 0.0421$ for all data. Selected bond lengths are given in the Figure captions (cf. Figures 1 and 4) and in the Supporting Information, Table S4. Further details of the crystal structure investigation may be obtained from the Fachinformationszentrum Karlsruhe, 76344 Eggenstein-Leopoldshafen, Germany (Fax: (+49) 7247–808–666; e-mail: crysdata@fiz-karlsruhe.de, or at http://www.fiz-karlsruhe.de/request for deposited data.html) on quoting the CSD number 425998.

Thermal analysis

The investigation of the thermal behavior was performed using a TGA/DSC apparatus (TGA/DSC1, Mettler Toledo GmbH, Schwerzenbach, Switzerland) and a TGA/SDTA device (TGA/SDTA851e, Mettler-Toledo GmbH, Schwerzenbach, Switzerland). In a flow of dry nitrogen, $Pd(NO_3)_2$ (about 11 mg) washed with *n*-hexane was placed in a corundum crucible and heated at a rate of 10 $Kmin^{-1}$ up to 1050 °C. For $Pd(CH_3SO_3)_2$, a sample was dried as far as possible using a fine paper towel. For a measurement under N_2 atmosphere, 9.0 mg of the sample were filled in a corundum crucible; for investigations in an O_2 stream, 4.4 mg of $Pd(CH_3SO_3)_2$ were treated in the same way. The crucibles were heated at a rate of 10 $Kmin^{-1}$ up to 1050 °C. The data were base-line-corrected and the characteristic point was taken from the DTA and DSC curves, respectively. As confirmation of the assumed oxidation on palladium during the course of the decomposition reactions of $Pd(CH_3SO_3)_2$ under O_2, we heated elemental palladium in an O_2 stream with rate of 10 $Kmin^{-1}$ up to 1050 °C. The respective diagram is given in the Supporting Information, Figure S5. The collected data were processed using the software of the analyzer.[20]

X-ray powder diffraction

The adhesive nitric acid of the crude $Pd(NO_3)_2$ product was washed away with dried *n*-hexane in a glove box. The dried bulk material was ground and checked by means of X-ray powder diffraction techniques on a sample prepared in a glass capillary (diameter 0.5 mm). The measurement was performed with the help of the powder diffractometer STADIP (Stoe & Cie) using Cu-Kα radiation ($\lambda = 154.06$ pm). The diffraction data were processed with the WinXPow 2007 program package. The lattice parameters obtained from the diffractogram are: $a = 469.2(2)$ pm, $b = 594.5(3)$ pm, $c = 805.3(4)$ pm, $\beta = 105.85(4)^\circ$, $V = 216.1(2)$ Å^3. The experimental and the calculated diffractogram of $Pd(NO_3)_2$ are shown in the Supporting Information, Figure S3. Apart from some very small reflections at low 2θ values, both diffractograms match quiet well. The data were processed with the WINXPOW program.[21]

For $Pd(CH_3SO_3)_2$, the mother liquor could only be removed mechanically by wiping on a fine paper towel. Washing of the crystals and bulk material with other even non polar solvents leads to decomposition. Nevertheless, the adhesive acid could be removed sufficiently, so that the bulk material of $Pd(CH_3SO_3)_2$ could be ground and filled in a glass capillary (diameter 0.5 mm) for XRD powder diffraction. The diffraction data were collected using the STADIP diffractometer (Stoe & Cie) using Cu-Kα radiation ($\lambda =$ 154.06 pm) and processed with the WinXPow 2007 program package.[21] The lattice parameters obtained from the diffractogram are: $a = 480.2(1)$ pm, $b = 1091.2(2)$ pm, $c = 749.1(2)$ pm, $\beta = 102.66(2)^\circ$, $V = 382.9(2)$ Å^3. Besides several well-indexed sharp reflections for $Pd(CH_3SO_3)_2$, we only find small reflections for some unreacted palladium (Supporting Information, Figure S4). The data were processed with the WINXPOW program.[21]

Vibrational spectroscopy

The Raman spectra were measured (spectrometer FRA106, Bruker, Karlsruhe, Germany) on a number of selected crystals in a small glass tube. For the measurements of the IR spectra, a sample of the respective compound was mounted in a glove box to the sample holder of a FTIR spectrometer (PlatinumATR, Tensor 27, Bruker) and immediately measured. Previously, the nitrate was washed with *n*-hexane, while the methanesulfonate was cleaned mechanically by wiping with a soft paper towel. The IR data were processed with the OPUS 2.0.5 program.[22] The assignment of the observed vibrations was carried out based on theoretical investigations, which were performed for characteristic cut-offs of the solid state structures.

Theoretical investigations

For the calculations, two different fragments of the crystal structures were chosen. In the case of the nitrate we extracted

a $[(NO_3)_3Pd(NO_3)Pd(NO_3)_3]^{3-}$, which should clearly reveal the characteristics of the bidentate bridging nitrate group. For $Pd(CH_3SO_3)_2$, we selected a $[(CH_3SO_3)_2Pd(CH_3SO_3)_2Pd(CH_3SO_3)_2]^{2-}$ anion with two bidentate bridging $CH_3SO_3^-$ groups. A full geometry optimization for both fragments has been performed within density functional theory (DFT) using the B3LYP functional for exchange and correlation. A 6-31+G(d) basis set for S, O, C, and H was used, while pseudopotentials were adopted for Pd (PP-cc-pVDZ). Throughout the study, the Gaussian 09 program package was used.[23] For the comparison with the experimental data, we extracted the data for the respective bridging anions. The calculations were done without symmetry restrictions, thus in case of the $[PdO_4]$ moieties and the bridging $CH_3SO_3^-$ groups we calculated more distances than found experimentally. For comparison, the very similar theoretical values have been merged.

Acknowledgements

Financial support of the Deutsche Forschungsgemeinschaft is gratefully acknowledged. J.B. is thankful for a stipend of the Stiftung der Metallindustrie im Nordwesten. The authors want to thank Dr. Marc Schmidtmann for the collection of the X-ray data. Furthermore we thank Mrs. Regina Stötzel and Prof. Claudia Wickleder (both University of Siegen) for measuring the Raman spectra. The simulations were performed at the HPC Cluster HERO, located at the University of Oldenburg (Germany) and funded by the DFG through its Major Research Instrumentation Programme (INST 184/108-1 FUGG) and the Ministry of Science and Culture (MWK) of the Lower Saxony State.

Keywords: X-ray diffraction · methanesulfonate · nitrate · palladium · theoretical investigations

[1] M. S. Wickleder, *Z. Anorg. Allg. Chem.* **2001**, *627*, 2112 – 2114.
[2] M. Pley, M. S. Wickleder, *Z. Anorg. Allg. Chem.* **2004**, *630*, 1036 – 1039.
[3] a) T. Dahmen, P. Rittner, S. Boeger-Seidl, R. Gruehn, *J. Alloys Compd.* **1994**, *216*, 11 – 19; b) J. Bruns, A. Fischer, M. S. Wickleder, unpublished results.
[4] J. Bruns, M. Eul, R. Pöttgen, M. S. Wickleder, *Angew. Chem. Int. Ed.* **2012**, *51*, 2204 – 2207; *Angew. Chem.* **2012**, *124*, 2247 – 2250.
[5] J. Bruns, O. Niehaus, R. Pöttgen, M. S. Wickleder, *Chem. Eur. J.* **2014**, *20*, 811 – 814.
[6] J. Bruns, T. Klüner, M. S. Wickleder, *Chem. Asian J.* **2014**, *9*, 1594 – 1600.
[7] a) C. Logemann, D. Gunzelmann, T. KLüner, J. Senker, M. S. Wickleder, *Chem. Eur. J.* **2012**, *18*, 15495 – 155503; b) C. Logemann, J. Witt, D. Gunzelmann, J. Senker, M. S. Wickleder, *Z. Anorg. Allg. Chem.* **2012**, *638*, 2053 – 2061; c) C. Logemann, K. Rieß, M. S. Wickleder, *Chem. Asian J.* **2012**, *7*, 2912 – 2920; d) see Ref. [3].
[8] M. S. Wickleder, F. Gerlach, S. Gagelmann, J. Bruns, M. Fenske, K. Al-Shamery, *Angew. Chem. Int. Ed.* **2012**, *51*, 2199 – 2203; *Angew. Chem.* **2012**, *124*, 2242 – 2246.
[9] a) Y. Laligant, G. Férey, A. Le Bail, *Mater. Res. Bull.* **1991**, *26*, 269 – 275; b) S. P. Khranenko, I. A. Baidina, S. A. Gromilov, *J. Struct. Chem.* **2007**, *48*, 1152 – 1155.
[10] C. Logemann, T. Klüner, M. S. Wickleder, *Z. Anorg. Allg. Chem.* **2012**, *638*, 1468 – 1472.
[11] M. D. Gernon, M. Wu, T. Buszta, P. Janney, *Green Chem.* **1999**, *1*, 127 – 140.
[12] a) S. P. Khranenko, I. A. Baidina, S. A. Gromilov, A. V. Belyaev, *J. Struct. Chem.* **2000**, *41*, 709 – 712; b) S. P. Khranenko, I. A. Baidina, S. A. Gromilov, A. V. Belyaev, *J. Struct. Chem.* **2009**, *50*, 361 – 364; c) S. P. Khranenko, I. A. Baidina, S. A. Gromilov, A. V. Belyaev, *J. Struct. Chem.* **2005**, *46*, 1060 – 1065.
[13] G. R. Desiraju, *Acc. Chem. Res.* **1991**, *24*, 290 – 296.
[14] G. A. Jeffrey, *An Introduction to Hydrogen Bonding*, Oxford University Press, **1997**.
[15] D. Avci, A. Başoğlu, Y. Atalay, *Z. Naturforsch. A* **2008**, *63*, 712 – 720.
[16] K. Dehnicke, J. Strähle, *Chem. Ber.* **2006**, *139*, 1502 – 1510.
[17] G. M. Sheldrick, *Acta Crystallogr. Sect. A* **2008**, *64*, 112 – 122.
[18] *SADABS*, Bruker, Madison, Wisconsin, USA, **2001**.
[19] *TWINABS*, Bruker, Madison, Wisconsin, USA, **2001**.
[20] *Star^e V 9.3*, Mettler-Toledo GmbH, Schwerzenbach, Switzerland, **2009**.
[21] *inXPOW 2007*, Stoe & Cie, Darmstadt, Germany, **2006**.
[22] *OPUS 6.5*, Bruker Optik GmbH, Germany, **2009**.
[23] Gaussian 09, Revision D.01, M. J. Frisch, G. W. Trucks, H. B. Schlegel, G. E. Scuseria, M. A. Robb, J. R. Cheeseman, G. Scalmani, V. Barone, B. Mennucci, G. A. Petersson, H. Nakatsuji, M. Caricato, X. Li, H. P. Hratchian, A. F. Izmaylov, J. Bloino, G. Zheng, J. L. Sonnenberg, M. Hada, M. Ehara, K. Toyota, R. Fukuda, J. Hasegawa, M. Ishida, T. Nakajima, Y. Honda, O. Kitao, H. Nakai, T. Vreven, J. A. Montgomery, Jr., J. E. Peralta, F. Ogliaro, M. Bearpark, J. J. Heyd, E. Brothers, K. N. Kudin, V. N. Staroverov, R. Kobayashi, J. Normand, K. Raghavachari, A. Rendell, J. C. Burant, S. S. Iyengar, J. Tomasi, M. Cossi, N. Rega, J. M. Millam, M. Klene, J. E. Knox, J. B. Cross, V. Bakken, C. Adamo, J. Jaramillo, R. Gomperts, R. E. Stratmann, O. Yazyev, A. J. Austin, R. Cammi, C. Pomelli, J. W. Ochterski, R. L. Martin, K. Morokuma, V. G. Zakrzewski, G. A. Voth, P. Salvador, J. J. Dannenberg, S. Dapprich, A. D. Daniels, Ö. Farkas, J. B. Foresman, J. V. Ortiz, J. Cioslowski, D. J. Fox, Gaussian, Inc., Wallingford CT, **2009**.

Received: September 21, 2014
Published online on November 27, 2014